A&A, 706, L21 (2026)
https://doi.org/10.1051/0004-6361/202558064

Astronomy & Astrophysics

LETTER TO THE EDITOR

Coherent bulk motions in a weakly turbulent merging Coma cluster

E. Gatuzz[1,⋆], J. Sanders[1], A. Liu[1,2], A. Fabian[3], C. Pinto[4], D. Eckert[5], and S. Walker[6]

[1] Max-Planck-Institut für extraterrestrische Physik, Gießenbachstraße 1, 85748 Garching, Germany
[2] Institute for Frontiers in Astronomy and Astrophysics, Beijing Normal University, Beijing 102206, China
[3] Institute of Astronomy, Madingley Road, Cambridge CB3 0HA, UK
[4] INAF – IASF Palermo, Via U. La Malfa 153, I-90146 Palermo, Italy
[5] Department of Astronomy, University of Geneva, Ch. d'Ecogia 16, CH-1290 Versoix, Switzerland
[6] Department of Physics and Astronomy, University of Alabama in Huntsville, Huntsville, AL 35899, USA

Received 11 November 2025 / Accepted 31 January 2026

ABSTRACT

The hot gas permeating galaxy clusters – the intracluster medium (ICM) – is a key tracer of their assembly history and internal dynamics. Understanding the motion of this gas provides critical insight into processes such as mergers, turbulence, and energy dissipation in the largest gravitationally bound structures in the Universe. The Coma cluster is a nearby, massive system long suspected to be dynamically disturbed. Previous high-resolution X-ray spectroscopy with the XRISM mission revealed bulk motions in the cluster core and southern regions. Here we present new XRISM Resolve observations of a northern region in Coma, which reveal a coherent velocity gradient of nearly 530 km/s across the cluster from south to north. We find that the hot gas in this northern region exhibits modest line-of-sight motions and uniform thermodynamic properties, indicating relatively mild local disturbances. The consistent levels of turbulence throughout the cluster suggest that the energy from a past merger has been distributed on large scales. These findings provide compelling evidence for an off-axis merger event and demonstrate how high-resolution X-ray spectroscopy can uncover subtle dynamical signatures in the ICM, offering important constraints for simulations of cluster evolution.

Key words. galaxies: clusters: intracluster medium – galaxies: clusters: individual: Coma – X-rays: galaxies: clusters

1. Introduction

Galaxy clusters grow through mergers and accretion, processes that drive turbulent motions and bulk flows in the intracluster medium (ICM), influencing pressure support, metal transport, and energy redistribution (Heinz et al. 2010; Schmidt et al. 2017; ZuHone et al. 2018; Vazza et al. 2021). Over the past decade, indirect constraints from X-ray and Sunyaev-Zel'dovich surface-brightness fluctuations have provided statistical insights into the amplitude and spectrum of ICM motions in nearby clusters, including Coma (Churazov et al. 2012; Zhuravleva et al. 2018). Direct velocity measurements, however, have been limited by spectral resolution, and calibration uncertainties (Zhuravleva et al. 2014; Pinto et al. 2015; Liu et al. 2018), until Hitomi resolved line-of-sight gas motions in the Perseus cluster, demonstrating that Active Galactic Nucleus (AGN) driven velocity fluctuations on ∼10–50 kpc scales are subsonic yet sufficiently energetic to balance radiative cooling in the ICM (Hitomi Collaboration 2016).

The launch of XRISM in 2023 has enabled high-resolution spectroscopy across cluster-wide scales. Observations of Abell 2029 show a nearly low-turbulence ICM with subsonic velocity dispersions (169 ± 10 km/s) and a nonthermal pressure fraction of ∼2.6%, while Centaurus exhibits modest bulk flows (130−310 km/s) with similarly highly subsonic velocities XRISM Collaboration (2025a,b). The Coma cluster (z = 0.02333, Bilton & Pimbblet 2018), a massive nearby cluster undergoing complex mergers, presents a unique environment for studying large-scale gas motions. It exhibits multiple signatures of ongoing dynamical activity: a disturbed X-ray morphology, a giant radio halo, and substructures associated with the dominant galaxies NGC 4874 and NGC 4889, which exhibit a velocity offset of ∼700 km/s (Fitchett & Webster 1987; Briel et al. 1992; White et al. 1993; Adami et al. 2005). Infalling groups such as NGC 4839 and NGC 4911/4921 further complicate the cluster's velocity field Adami et al. (2005). Recent XRISM observations of the core and southern regions revealed substantial bulk motions alongside subsonic velocity dispersions, indicating subsonic turbulence and a dynamically evolved state XRISM Collaboration (2025c). Here we present new XRISM Resolve observations of a northern region, extending coverage beyond performance verification pointings.

2. XRISM data reduction

The northern Coma cluster was observed with *XRISM*/Resolve on 2025 January 14 (ObsID 201114010) for a net exposure of 144.8 ks after standard filtering. The energy resolution was 4.51 ± 0.02 eV at 5.9 keV, corresponding to a velocity uncertainty <10 km/s, well below the statistical errors.

Spectra were extracted for the full field of view (FOV) and for four quadrants (NE, NW, SE, and SW) to probe spatial variations. The non-X-ray background (NXB) contributed <8% of the counts, and Auxiliary Response Files (ARFs) were computed using *Chandra* 2–7 keV images with point sources removed. Point Spread Function (PSF) scattering effects were modeled with `xrtraytrace`. For further details on the data reduction, including event selection, response generation, and quadrant extraction, see Appendix A.

⋆ Corresponding author: `egatuzz@mpe.mpg.de`

Table 1. Best-fit parameters in the 2–10 keV energy band for all regions analyzed.

Region	Temperature (keV)	Abundance (Solar)	Redshift z	$v_{\rm bulk}$ (km/s)	Turbulent velocity σ_v (km/s)	*norm*	C-stat/d.o.f.
FOV	8.14 ± 0.36	0.28 ± 0.03	0.02273 ± 0.00009	-199 ± 26	167 ± 39	0.195 ± 0.004	1779/1874
NE	8.55 ± 0.83	0.38 ± 0.08	0.02288 ± 0.00030	-155 ± 87	444 ± 256	0.183 ± 0.009	1017/1261
NW	8.20 ± 0.73	0.25 ± 0.06	0.02258 ± 0.00019	-243 ± 55	118 ± 88	0.185 ± 0.009	1114/1287
SE	7.60 ± 0.62	0.28 ± 0.05	0.02257 ± 0.00028	-246 ± 82	303 ± 141	0.101 ± 0.009	1154/1360
SW	8.05 ± 0.65	0.27 ± 0.06	0.02265 ± 0.00020	-223 ± 58	150 ± 85	0.183 ± 0.008	1091/1308

Notes. $v_{\rm bulk}$ calculation in km/s includes heliocentric correction.

3. Spectral fitting

Spectral fitting was performed in the 2–10 keV band using *xspec* v12.14.1 and Cash statistics (Cash 1979). The ICM was modeled with a single-temperature `bapec` component including thermal and turbulent broadening. Redshift, temperature, abundance (proto-solar, Lodders et al. 2009), velocity dispersion, and normalization were free parameters. Galactic absorption was included via `tbabs` with $N_{\rm H} = 8.66 \times 10^{20}$ cm^{-2} (Willingale et al. 2013), and all velocities were corrected to the heliocentric frame. To test for multi-temperature structures, two-temperature (`bapec+bapec`) and lognormal (`blognorm`, Gatuzz et al. 2022) models were also applied. The NXB contributed <8% of counts and had negligible effect on velocity measurements. For full technical details, including model configurations, parameter tying, and Markov Chain Monte Carlo (MCMC) sampling, see Appendix B.

4. Results and discussion

We performed spectral fitting over the full *XRISM* Resolve FOV using three ICM models: a single-temperature `bapec`, a two-temperature `bapec+bapec`, and a lognormal temperature distribution with `blognorm`. To test whether complex models were statistically warranted, we used a simulation-based $\Delta cstat$ method following Buchner & Boorman (2023). For each case, 1000 spectra were simulated from the simpler model, and the 99th percentile of the resulting $\Delta cstat$ distribution defined the critical threshold ($\Delta cstat_{\rm crit}$) corresponding to a 1% false-positive rate. We found $\Delta cstat_{\rm crit} = 6.38$ for `2-bapec` and 3.75 for `blognorm`. Neither model exceeded these thresholds, confirming that a single-temperature component adequately describes the data. The `blognorm` model only yielded an upper limit on the width parameter, and the second component in the two-temperature fit was consistent with zero. This supports a uniform thermal structure, consistent with previous findings in the Coma outskirts (Arnaud et al. 2001; Sanders et al. 2020; XRISM Collaboration 2025c).

Best-fit parameters for the `bapec` model obtained via MCMC are listed in Extended Data Table 1. Convergence diagnostics confirmed robust mixing ($\tau \lesssim 1$), yielding $\gtrsim 3.8 \times 10^7$ effective samples. The best-fit redshift corresponds to a bulk velocity of $v_{\rm bulk} = -199 \pm 26$ km/s and a velocity dispersion of $\sigma_v = 167 \pm 39$ km/s. These values agree with *XMM-Newton* results ($z = 0.023$, $v = -57 \pm 150$ km/s; Sanders et al. 2020) and are notably lower than those observed in the Coma core (-450 ± 15 km/s) and southern regions (-730 ± 30 km/s; Fig. 1), confirming significant large-scale gas motions across the cluster.

To examine spatial variations in the thermodynamic and kinematic properties of the ICM, the *XRISM* Resolve FOV was divided into four quadrants: northeast (NE), northwest (NW), southeast (SE), and southwest (SW). Each region contains ~200 counts in the Fe XXV–XXVI complex (6.4–6.9 keV), sufficient to constrain line centroids and measure velocity dispersions, albeit with large statistical uncertainties due to limited counts. Spectra were fit independently using a single-temperature `bapec` model following XRISM Collaboration (2025c), with parameter uncertainties explored through MCMC sampling. The best-fit results are listed in Table 1, and Fig. 2 shows the corresponding bulk and turbulent velocities. Bulk velocities range from $v_{\rm bulk} = -246$ to -155 km/s, with 1σ uncertainties of $\lesssim$100 km/s. Measured velocity dispersions span $\sigma_v = 118$–444 km/s, reflecting the limited photon statistics rather than intrinsic variability. Temperatures are consistent within $kT = 7.60$–8.55 keV, and Fe abundances lie between $Z = 0.25$–0.38 (proto-solar). Overall, no significant spatial gradients are detected, indicating that the ICM in this region is thermally and kinematically uniform within current uncertainties.

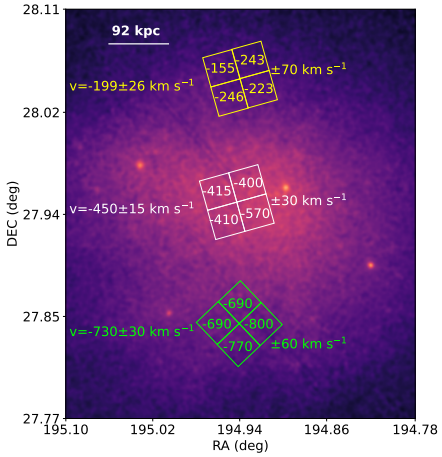

Fig. 1. Line-of-sight bulk velocities ($v_{\rm bulk}$) for the Coma cluster: northern region (yellow) and center-south (white-green; XRISM Collaboration 2025c). Values are shown for the full FOV and quadrants, overlaid on the XMM-Newton X-ray image (Sanders et al. 2020). Quadrant points include mean uncertainties.

We tested the spatial uniformity of velocity, velocity dispersion, temperature, and metallicity across the four quadrants by comparing each parameter to a constant model defined by the inverse-variance weighted mean. Reduced χ^2 and p-value analyses, along with the largest deviations from the mean, showed no significant departures from uniformity: 0.52σ for $v_{\rm bulk}$, 0.90σ for σ_v, 0.56σ for kT, and 0.78σ for Z. These results indicate consistency across the field, though moderate intrinsic variations may remain undetected within current uncertainties. To further quantify possible small-scale inhomogeneities, we applied an MCMC analysis modeling the total variance as $\sigma^2_{\rm tot,i} = \sigma^2_{\rm err,i} + \sigma^2_{\rm intr}$. The

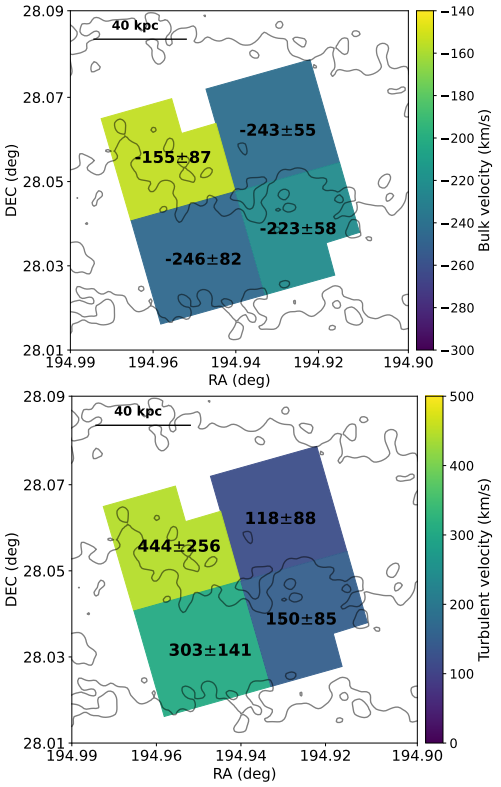

Fig. 2. Velocity maps obtained for the Coma cluster. *Top panel*: Bulk velocities ($v_{\rm bulk}$) obtained from the XRISM Resolve spectra. *Bottom panel*: Turbulent velocities (σ_v). The *Chandra* contours for the broad-band energy range (0.5–7 keV) are included.

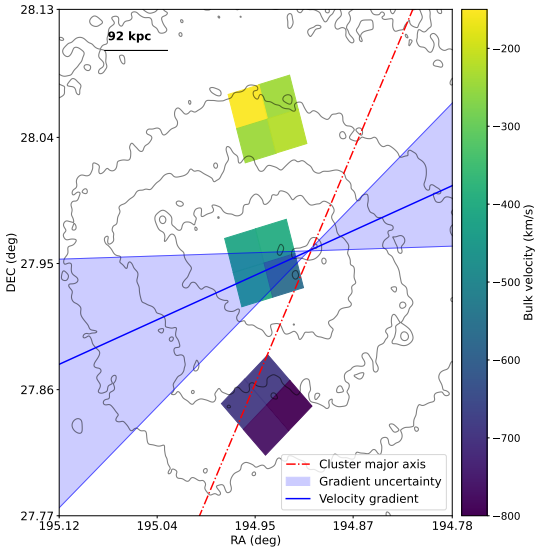

Fig. 3. Spatial distribution of Coma ICM line-of-sight velocities. XRISM Resolve pointings (north, center, and south) are divided into quadrants (NE, NW, SE, and SW) and color-coded by $v_{\rm bulk}$. Smoothed X-ray contours show gas density; the blue line indicates the best-fit velocity gradient (shaded region = uncertainty); and the dashed red line marks the cluster major axis (PA = 65°). The plot highlights a coherent large-scale velocity shear slightly misaligned with the cluster elongation.

ICM bulk velocity is consistent across all regions, with a common mean of $v_{\rm bulk} = -226 \pm 33$ km/s and negligible intrinsic scatter ($\sigma_I < 0.01$). The velocity dispersion, temperature, and metallicity show mild variations, with $\sigma_v = 174 \pm 55$ km/s, $kT = 8.03 \pm 0.35$ keV, and $Z = 0.28 \pm 0.03\ Z_\odot$, all with $\sigma_I < 10$. Overall, the ICM appears homogeneous on the Resolve scale, with only subtle, percent-level fluctuations consistent with the data.

To characterize the ICM velocity structure, we used the mean line-of-sight velocities from the three XRISM Resolve pointings (north, center, and south). Projected positions relative to the cluster center ($\mathrm{RA}_0 = 12^{\rm h}59^{\rm m}46^{\rm s}$, $\mathrm{Dec}_0 = +27°56'00''$) were converted to kiloparsec, and the velocity field was modeled as a linear plane:

$$v(x, y) = v_0 + a\,x + b\,y, \tag{1}$$

with v_0 the central velocity and (a, b) the gradients along Right ascension (RA) and Declination (Dec). The fit yields $a = 0.016$ km/s/kpc and $b = 4.06$ km/s/kpc, giving a total gradient $|\nabla v| = 4.06$ km/s/kpc oriented $\theta = 22.3 \pm 20.6°$ east of RA, or $-42.7°$ relative to the cluster major axis. This indicates a coherent, large-scale velocity shear across the ICM, providing the first high-resolution spectroscopic measurement of bulk motions in Coma over multiple scales, extending earlier XMM-Newton results (Sanders et al. 2020). While the orientation is indicative given limited sampling, this direct gradient measurement offers a complementary view of ICM dynamics pending the full velocity structure function analysis in a forthcoming study.

To assess the local dynamical state of the ICM, we compared XRISM Resolve line-of-sight velocities with the redshifts of seven cluster member galaxies within the northern FOV (Michard & Andreon 2008; den Brok et al. 2011; Eisenhardt et al. 2007). The galaxy sample has a mean redshift $\langle z_{\rm gal}\rangle = 0.0250$ ($\langle v_{\rm gal}\rangle = 7508$ km/s) and standard deviation $\sigma_{z,\rm gal} = 0.0034$ ($\sigma_{v,\rm gal} = 1021$ km/s). A simple z-test shows the XRISM full-FOV velocity differs by only 0.68σ from the galaxy mean, indicating no strong deviation within this small sample. To account for the large intrinsic galaxy scatter, we performed a Bayesian MCMC analysis modeling the ICM and galaxy mean velocities and the intrinsic galaxy dispersion. This yields a median velocity offset of $\Delta V = \mu_{\rm ICM} - \mu_{\rm gal} = -711^{+68}_{-72}$ km/s, with the 68% credible interval excluding zero, indicating a statistically significant bulk motion of the ICM relative to the local galaxy population. These results suggest the ICM in the northern FOV is either part of a distinct kinematic substructure or exhibits coherent bulk flows, reflecting a dynamically active state.

We estimated the contribution of turbulent motions to the ICM pressure by computing the adiabatic sound speed c_s, the 3D Mach number $\mathcal{M}_{\rm 3D} = \sqrt{3}\sigma_v/c_s$, the turbulent-to-thermal energy ratio $E_{\rm turb}/E_{\rm therm} = (\gamma/2)\mathcal{M}^2_{\rm 3D}$, and the kinetic pressure fraction $P_{\rm turb}/P_{\rm tot} = \left(1 + 3/\gamma\,\mathcal{M}^2_{\rm 3D}\right)^{-1}$. Here, σ_v is the line-of-sight velocity dispersion, which quantifies random gas motions that contribute to pressure support, while coherent bulk velocities are excluded. We adopted $\gamma = 5/3$, $\mu = 0.61$ and the best-fit ICM temperature from the spectral analysis. Uncertainties were propagated assuming Gaussian errors on σ_v and kT.

For the northern Coma FOV, we find $\mathcal{M}_{\rm 3D} = 0.197 \pm 0.046$, $E_{\rm turb}/E_{\rm therm} = 0.032 \pm 0.015$, and $P_{\rm turb}/P_{\rm tot} = 0.021 \pm 0.010$, indicating subsonic turbulence with only ~2% nonthermal pressure support. These results are in excellent agreement with recent XRISM measurements: A2029 ($M_{\rm 3D} = 0.22$, $P_{\rm kin}/P_{\rm tot} = 2.6\%$), Centaurus ($M_{\rm 3D} \lesssim 0.2$, $E_{\rm turb}/E_{\rm therm} \sim 3\%$), Perseus ($M_{\rm 3D} \sim 0.1 - 0.3$, $P_{\rm kin}/P_{\rm tot} \sim 1 - 5\%$), Coma Performance Verification (PV) pointings ($M_{\rm 3D} = 0.24 \pm 0.015$, $P_{\rm kin}/P_{\rm tot} = 3.1 \pm 0.4\%$), Ophiuchus ($M_{\rm 3D} = 0.16$, $P_{\rm kin}/P_{\rm tot} = 1.4\%$), and Abell 2319 ($M_{\rm 3D} = 0.49^{+0.23}_{-0.12}$, $P_{\rm kin}/P_{\rm tot} = 11.2^{+10.6}_{-4.7}\%$). Our Mach numbers and nonthermal pressure fractions are also

broadly consistent with indirect measurements based on X-ray and Sunyaev-Zeldovich (SZ) surface-brightness fluctuations, including Churazov et al. (2012) for Coma ($M_{3D} \sim 0.23$, $E_{turb}/E_{therm} \sim 3\%$), Zhuravleva et al. (2018) ($E_{turb}/E_{therm} \sim 5\%$), Dupourqué et al. (2024) ($M_{3D} \sim 0.4$, $P_{turb}/P_{tot} \sim 9\%$), and Romero et al. (2025) ($M_{3D} \sim 0.52$). Following the emission-measure–weighted definition adopted in XRISM collaboration papers (e.g., XRISM Collaboration 2025d), and consistent with the approach of Zhuravleva et al. (2012), we estimate the effective line-of-sight depth contributing to the X-ray emission in the northern Coma FOV to be ∼260 kpc. This value is in good agreement with the XRISM southern Coma pointing (XRISM Collaboration 2025c) and is significantly higher than in more centrally peaked systems such as Centaurus ($\lesssim$50 kpc, XRISM Collaboration 2025c) or M87 (∼5–35 kpc, XRISM Collaboration 2025d). While differences in line-of-sight depth can affect the inferred velocity dispersion, the Coma ICM shows coherent large-scale bulk motions with locally subsonic turbulence and modest nonthermal pressure support.

5. The complex ICM dynamics of the Coma cluster

In addition to subsonic turbulence, we detect coherent bulk motions in Coma. Combining our northern pointing with previous XRISM measurements of the central and southern regions (XRISM Collaboration 2025c) reveals line-of-sight velocities of −730 km/s (south), −450 km/s (core), and −199 km/s (north), corresponding to a ∼530 km/s gradient across several hundred kiloparsecs (Figure 1). Fitting a planar velocity model yields a gradient of ∼4.1 km/s/kpc, oriented 22 ± 21° east of the RA axis, slightly misaligned with the cluster elongation, indicating a coherent velocity shear. Subdividing each field into quadrants produces similar trends, though uncertainties limit sensitivity to small-scale variations.

Compared with other nearby clusters observed with XRISM, Coma displays distinctive kinematics. Its northern line-of-sight velocity dispersion ($\sigma_v = 167 \pm 39$ km/s) is comparable to relaxed systems such as the A2029 core (XRISM Collaboration 2025a), yet unlike those clusters, Coma exhibits a global velocity gradient spanning hundreds of kiloparsecs. Despite this, the Mach number and nonthermal pressure fraction remain low, consistent with a locally relaxed ICM. These features are naturally explained by an off-axis merger, producing large-scale bulk flows while maintaining near-uniform thermodynamic and kinematic properties within each pointing. Hydrodynamical simulations and recent theoretical studies (Biffi et al. 2011, 2022; Vazza & Brunetti 2026; Groth et al. 2025) support this scenario, showing that mergers can generate extended velocity gradients without strongly enhancing local turbulence. Together, these findings reinforce our observational conclusion that the Coma ICM exhibits coherent bulk motions over hundreds of kiloparsecs while maintaining relatively subsonic velocities and near-uniform properties within individual XRISM pointings.

6. Conclusions and summary

We analyzed the velocity structure of the Coma galaxy cluster using new *XRISM*/Resolve observations of a region north of the cluster core. The spectrum of the ICM is well described by a single-temperature model, with no significant improvement obtained from more complex descriptions. For the entire FOV, we measure a line-of-sight bulk velocity of $v_{bulk} = (-199 \pm 26)$ km/s and a velocity dispersion of $\sigma_v = (167 \pm 39)$ km/s. Dividing the field into four quadrants reveals uniform thermodynamic properties and subsonic velocity dispersions, confirming the absence of strong local disturbances. The ICM redshift is consistent with that of the cluster member galaxies detected in the same region, suggesting that the hot gas and galaxies share a common dynamical state. From these measurements, we derive a 3D Mach number of $\mathcal{M}_{3D} = 0.197 \pm 0.046$, corresponding to a turbulent-to-thermal energy ratio of $(3.2 \pm 1.5)\%$ and a kinetic pressure fraction of $(2.1 \pm 0.5)\%$ of the total ICM pressure.

When combined with previous *XRISM* observations of the Coma core and southern regions, our measurements reveal a coherent velocity gradient of ∼4.06 km/s/kpc (∼530 km/s) across the cluster from south to north), oriented 22.3° ± 20.6° east of the right ascension axis. This large-scale shear, together with the uniform velocity dispersion across the pointings, provides direct evidence for an off-axis merger event that generated coherent bulk flows while leaving the local ICM relatively relaxed. The derived subsonic motions and modest nonthermal pressure support indicate that Coma is currently in a late-stage post-merger phase characterized by ordered large-scale flows. Overall, these results establish Coma as a benchmark for studies of cluster dynamics and demonstrate the capability of high-resolution X-ray spectroscopy to map multi-scale gas motions in the ICM.

References

Adami, C., Biviano, A., Durret, F., & Mazure, A. 2005, A&A, 443, 17
Arnaud, M., Aghanim, N., Gastaud, R., et al. 2001, A&A, 365, L67
Biffi, V., Dolag, K., & Böhringer, H. 2011, MNRAS, 413, 573
Biffi, V., ZuHone, J. A., Mroczkowski, T., Bulbul, E., & Forman, W. 2022, A&A, 663, A76
Bilton, L. E., & Pimbblet, K. A. 2018, MNRAS, 481, 1507
Briel, U. G., Henry, J. P., & Boehringer, H. 1992, A&A, 259, L31
Buchner, J., & Boorman, P. 2023, in Handbook of X-ray and Gamma-ray Astrophysics, 150
Cash, W. 1979, ApJ, 228, 939
Churazov, E., Vikhlinin, A., Zhuravleva, I., et al. 2012, MNRAS, 421, 1123
den Brok, M., Peletier, R. F., Valentijn, E. A., et al. 2011, MNRAS, 414, 3052
Dupourqué, S., Clerc, N., Pointecouteau, E., et al. 2024, A&A, 687, A58
Eisenhardt, P. R., De Propris, R., Gonzalez, A. H., et al. 2007, ApJS, 169, 225
Fitchett, M., & Webster, R. 1987, ApJ, 317, 653
Foster, A., Smith, R., & Brickhouse, N. S. 2019, Am. Astron. Soc. Meeting Abstr., 233, 251.05
Gatuzz, E., Sanders, J. S., Canning, R., et al. 2022, MNRAS, 513, 1932
Groth, F., Valentini, M., Seidel, B. A., et al. 2025, ArXiv e-prints [arXiv:2507.02041]
Heinz, S., Brüggen, M., & Morsony, B. 2010, ApJ, 708, 462
Hitomi Collaboration (Aharonian, F., et al.) 2016, Nature, 535, 117
Hitomi Collaboration (Aharonian, F., et al.) 2018, PASJ, 70, 12
Kaastra, J. S., & Bleeker, J. A. M. 2016, A&A, 587, A151
Liu, A., Yu, H., Diaferio, A., et al. 2018, ApJ, 863, 102
Lodders, K., Palme, H., & Gail, H.-P. 2009, Landolt Börnstein, 4B, 712
Michard, R., & Andreon, S. 2008, A&A, 490, 923
Pinto, C., Sanders, J. S., Werner, N., et al. 2015, A&A, 575, A38
Romero, C. E., Gaspari, M., Schellenberger, G., et al. 2025, ApJ, 985, 248
Sanders, J. S., Dennerl, K., Russell, H. R., et al. 2020, A&A, 633, A42
Schmidt, W., Byrohl, C., Engels, J. F., Behrens, C., & Niemeyer, J. C. 2017, MNRAS, 470, 142
Vazza, F., & Brunetti, G. 2026, A&A, 705, A129
Vazza, F., Wittor, D., Brunetti, G., & Brüggen, M. 2021, A&A, 653, A23
White, S. D. M., Briel, U. G., & Henry, J. P. 1993, MNRAS, 261, L8
Willingale, R., Starling, R. L. C., Beardmore, A. P., Tanvir, N. R., & O'Brien, P. T. 2013, MNRAS, 431, 394
XRISM Collaboration (Audard, M., et al.) 2025a, PASJ, 77, S242
XRISM Collaboration (Audard, M., et al.) 2025b, Nature, 638, 365
XRISM Collaboration (Audard, M., et al.) 2025c, ApJ, 985, L20
XRISM Collaboration (Audard, M., et al.) 2025d, ArXiv e-prints [arXiv:2512.06596]
Zhuravleva, I., Churazov, E., Kravtsov, A., & Sunyaev, R. 2012, MNRAS, 422, 2712
Zhuravleva, I., Churazov, E., Schekochihin, A. A., et al. 2014, Nature, 515, 85
Zhuravleva, I., Allen, S. W., Mantz, A., & Werner, N. 2018, ApJ, 865, 53
ZuHone, J. A., Miller, E. D., Bulbul, E., & Zhuravleva, I. 2018, ApJ, 853, 180

Appendix A: Detailed data reduction

The *XRISM*/Resolve observation of the Coma northern offset region (ObsID 201114010) was performed on 2025 January 14. Data reduction followed standard *XRISM* procedures (XRISM Collaboration 2025a,b,c) using HEASoft v6.34 and XRISM `CalDB` release 20241115. Events during South Atlantic Anomaly passages, Earth occultation, and low elevation ($< 20°$) from the sunlit limb were excluded, yielding a net exposure of 144.8 ks.

The onboard ^{55}Fe calibration source provided an energy resolution of 4.51 ± 0.02 eV at 5.9 keV and an energy-scale offset < 0.1 eV, corresponding to a velocity uncertainty < 10 km/s. Spectra were extracted using high-resolution primary events (ITYPE=0), excluding pixel 27 due to gain instability. The 2–10 keV count rate was 0.0697 ± 0.0007 cts/s, totaling $\sim$ 10100 counts, and spectra were optimally binned to one count per channel (Kaastra & Bleeker 2016).

Non-X-ray background spectra were generated using `rslnxbgen` from the Night Earth database, contributing $< 8\%$ of the total counts. Response files were generated with `rslmkrmf` and `xaarfgen`, adopting the "split-matrix" configuration for electron-loss continuum. ARFs were computed from a 2–7 keV *Chandra* ACIS-I image (six observations, 960 ks total) with point sources removed via `wavdetect`.

To investigate spatial variations, spectra and ARFs were extracted for four quadrants (NE, NW, SE, SW), each containing sufficient counts in the Fe K complex for velocity measurements. PSF scattering between quadrants was modeled with `xrtraytrace`, confirming negligible contamination between regions (less than 10%). This detailed data reduction ensures robust measurements of bulk velocities and turbulent line broadening across the northern Coma field.

Appendix B: Detailed spectral fitting

Spectral fitting was carried out in the 2–10 keV band using *xspec* v12.14.1 and Cash statistics (Cash 1979). We modeled the ICM with three approaches:

1. Single-temperature (`bapec` v3.0.9, Foster et al. 2019), including thermal and turbulent broadening calibrated from *Hitomi* Perseus results (Hitomi Collaboration 2018). Free parameters were temperature, redshift, abundance (protosolar, Lodders et al. 2009), velocity dispersion σ_v, and normalization.
2. Two-temperature (`bapec+bapec`), with redshift, abundance, and σ_v tied between components.
3. Continuous temperature distribution (`blognorm`, Gatuzz et al. 2022), assuming a lognormal temperature distribution with free median temperature, width, and σ_v.

All models included Galactic absorption via `tbabs` with fixed $N_{\rm H} = 8.66 \times 10^{20}$ cm^{-2} (Willingale et al. 2013). NXB was modeled using the standard *XRISM* template comprising a power-law continuum and Gaussian fluorescence lines (Cr, Mn, Fe, Ni, Cu, Au), contributing $< 8\%$ of counts and having negligible impact on velocity or line-width measurements (XRISM Collaboration 2025a,b,c).

We explored parameter uncertainties with MCMC sampling using the Goodman-Weare algorithm (*xspec*), with 25 walkers and 2×10^6 steps (first 5×10^5 discarded), ensuring robust estimates of bulk velocities and turbulent line widths. Velocities were corrected to the heliocentric frame (+24.1 km/s). We adopt a flat ΛCDM cosmology with $\Omega_m = 0.3$, $\Omega_\Lambda = 0.7$, and $H_0 = 70$ km/s/Mpc. All reported errors correspond to 1σ unless otherwise stated.

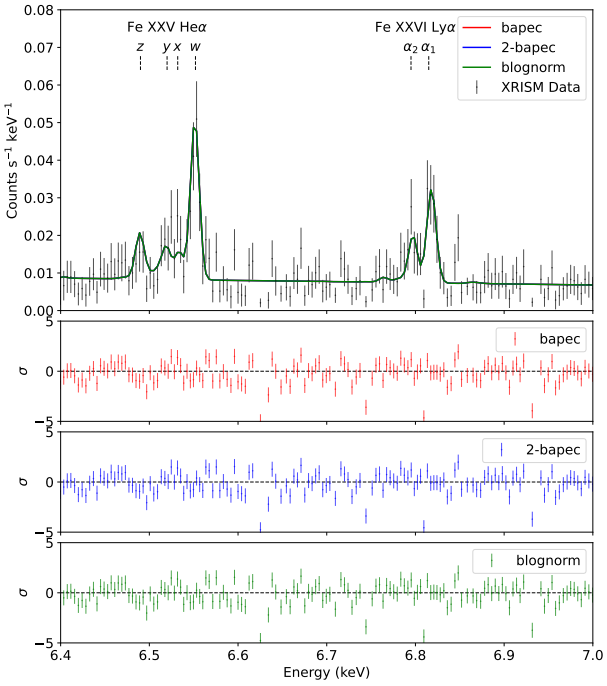

Fig. B.1. XRISM Resolve spectrum zoomed-in on the strongest Fe K-shell lines. He-like triplet components are shown: resonance (w), intercombination (x, y), and forbidden (z); Fe XXVI Lyα has α_1 and α_2 transitions. The spectrum is rebinned for clarity. Lower panels: Fit residuals for `bapec` (red), `2-bapec` (blue), and `blognorm` (green). Minor deviations in Fe XXVI α_2 and Fe XXV intercombination lines resemble those seen in Coma (southern and center pointings), A2029, and Centaurus (XRISM Collaboration 2025a,b,c).

Figure B.1 shows the Fe K-shell features with best-fit models and residuals. Minor deviations in the Fe XXVI Lyα_2 and Fe XXV intercombination lines-also seen in A2029 and Centaurus (XRISM Collaboration 2025a,c)–likely arise from residual calibration or atomic data systematics, which are being investigated through a broader cross-comparison effort.